Talanta 88 (2012) 115–120

Contents lists available at SciVerse ScienceDirect

Talanta

journal homepage: www.elsevier.com/locate/talanta

Synthesis and characterization of $InNbO_4$ nanopowder for gas sensors

C. Balamurugan[a], E. Vijayakumar[b], A. Subramania[b,*]

[a] Department of Industrial Chemistry, Alagappa University, Karaikudi-630 003, India
[b] Centre for Nanoscience and Technology, Pondicherry University, Puducherry-605 014, India

ARTICLE INFO

Article history:
Received 14 June 2011
Received in revised form 8 October 2011
Accepted 13 October 2011
Available online 26 November 2011

Keywords:
Nanopowder
$InNbO_4$
Gas sensor
Semiconductor
LPG gas
Niobium-citrate process

ABSTRACT

Indium niobate ($InNbO_4$) nanopowder was prepared by a comparatively low temperature niobium citrate complex process. The prepared $InNbO_4$ was characterized by thermal analysis, X-ray diffraction analysis (XRD), scanning electron microscopy (SEM), transmission electron microscopy (TEM), energy dispersive X-ray spectroscopy, diffuse reflectance spectroscopy (DRS), and impedance studies. It revealed that the well crystalline monoclinic $InNbO_4$ nanopowder was obtained at the calcination temperature of 600 °C. The average particle diameter was 22 nm. The optical band gap was found to be 2.66 eV. The temperature dependent conductivity obeyed Arrhenius relation. The activation energy of the conductivity process was calculated to be 0.43 eV. The gas sensing behaviour of the prepared $InNbO_4$ was studied by measuring the change in resistance of the sensor material as a function of various concentrations of the test gases such as liquid petroleum gas (LPG), ammonia (NH_3) and ethanol (C_2H_5OH) at their optimized operating temperature. $InNbO_4$ had a better sensitivity to LPG (0.97) and NH_3 (0.70) gas than ethanol (0.46). The sensor responses of $InNbO_4$ as a function of gas concentrations and with recovery time were also studied in detail.

1. Introduction

In_2O_3 has been found to possess gas sensing activity [1,2]. However, in order to enhance gas sensitivity and selectivity, various additives have been used. The additives could act as promoters, catalysts, surface sites for adsorption of oxygen and gases to be detected by promoting improvement of porosity of the gas sensing matrix. Earlier works reveal that a small amount of additives significantly affected both electrophysical and gas sensing characteristics of metal oxides. Noble metals or transition metals namely Pt, Ru, Fe, Mn, Ni, Al, Cr, Co, Bi, etc. had been used a dopant in In_2O_3 to improve gas sensing properties [3–5]. $InNbO_4$ based semiconductor materials have been attracted by many researchers due to its unique structural and important physical properties [6–8]. This can also be used as a key precursor for the ferroelectric perovskite, lead indium niobate, ($Pb(In_{1/2}\ Nb_{1/2})O_3$) for actuator, transducer and ultrasonic motor applications [9]. Indium niobate based materials were prepared by solid-state reactions of In_2O_3 and Nb_2O_5 at high calcination temperatures [10,11]. However, this preparation process had several disadvantages such as controlling the component homogeneity, crystal size, stoichiometric ratio, and formation of un-desirable phases. In the present investigation, monoclinic $InNbO_4$ nanopowder had been synthesized using niobium citrate complex process. This process yielded reactive powder with high purity, higher surface areas, fine particle size, high degree of crystallinity, and low temperature sinterability, compared to the powder prepared by conventional solid state reaction method. In addition, as the reactants are mixed in an aqueous solution, this method enabled to produce a good chemical homogeneity of the system. The prepared $InNbO_4$ nanopowder was studied with various characterization techniques such as XRD, SEM, TEM and impedance analysis. The gas sensing properties of the $InNbO_4$ nanopowder had been studied for different gases such as liquid petroleum gas (LPG), ammonia (NH_3) and ethanol (C_2H_5OH) at various operating temperatures. The response of $InNbO_4$ nanopowder as a function of gas concentrations and with recovery time was also studied.

2. Experimental

2.1. Synthesis of $InNbO_4$ nanopowder

$InNbO_4$ nanopowder was obtained by comparatively low temperature niobium citrate complex process using following two steps. The first step was the preparation of hydrated Nb_2O_5 from Nb_2O_5 [12]. Nb_2O_5 was dissolved in HF to form $[NbOF_5]^{2-}$ or $[NbF_7]^{2-}$ complex. A freshly prepared aqueous solution of ammonium oxalate was added in excess and then aqueous NH_3 was added drop by drop to get hydrous niobium oxide ($Nb_2O_5{\cdot}nH_2O$) as precipitated. The precipitate of hydrous oxide was filtered and washed

* Corresponding author. Tel.: +91 0413 2654980; fax: +91 0413 2654612.
E-mail address: a_subramania@yahoo.co.in (A. Subramania).

0039-9140/$ – see front matter © 2011 Elsevier B.V. All rights reserved.
doi:10.1016/j.talanta.2011.10.017

with 10% aqueous NH_3 solution by centrifugation to make the solution fluoride free hydrated Nb_2O_5. In the second step, the stoichiometry amount of hydrated Nb_2O_5 was dissolved in the aqueous solution of citric acid (2 mol/mol of niobium ion) with the addition of catalytic amount of hydrogen peroxide, to get clear yellow coloured peroxo-citro-niobate. The addition of H_2O_2 promoted the solubility of the hydrated niobiate in citric acid and also shortened the required dissolution time. The clear solution of peroxo-citro-niobiate was mixed with stoichiometric amount of indium nitrate (mole ratio of In/Nb = 1:1) with constant stirring. The pH of the final solution mixture was adjusted to 7 by addition of aqueous NH_3. This mixture was heated at about 200 °C to get a dried black fluffy mass. This dried mass was calcined at 600 °C for 2 h to get $InNbO_4$ nanopowder. The resultant product was collected and subjected into both physical characterization and gas sensor studies.

3. Structural characterization studies

The thermal decomposition of as-prepared $InNbO_4$ powder was studied by TG/DTA (Model: Pyris Diamond) analysis under air atmosphere from 30 to 900 °C at a heating rate of 10 °C/min. The crystalline phase of the $InNbO_4$ powder was identified by X-ray diffractometer (Model: X' Pert-pro) using Cu-Kα radiation as the sources and operated at 40 kV. The sample was scanned in the 2θ range of 20–60° with 0.02° step. Powder morphology was observed by using scanning electron microscopy (SEM) (Model: SN-3400N). Further, the particle size and crystalline quality of the synthesized powder were obtained using transmission electron microscopy (TEM) (Model: Philips CM-20) operated at 200 kV. The composition of the powder was obtained by energy dispersive X-ray spectroscopy (EDX) linked to the TEM system. For TEM investigation, sample was prepared from a sonicated suspension of the $InNbO_4$ powder in ethanol. A drop of the suspension was placed in a carbon coated copper grid. After evaporation of the ethanol, the remaining particles were viewed in the transmission electron microscope. The band gap energy of $InNbO_4$ nanopowder was determined from using UV–vis absorption spectra (Model: Varian, Cary-5000) equipped with a diffuse reflectance accessory. The surface area of $InNbO_4$ powder was measured the BET (Micrometrisics, ASAP 2020) nitrogen adsorption and desorption method at −196 °C. The electrical conductivity of the synthesized $InNbO_4$ nanopowder was studied by mixing $InNbO_4$ nanopowder with a few drop of polyvinyl alcohol solution and the mixture was pressed into a pellet of 10 mm diameter and 1.5–2.0 mm thickness using a die at 150 MPa. The pellet was then heat-treated at 400 °C to remove the residual polymer which helps to produce porous solid. Conductivity of pellet was measured with the help of stainless steel blocking electrodes using a computer-controlled Potentiostat/Galvanostat (Model: Autolab type III) in the frequency range of 1 Hz–500 kHz at 30–175 °C.

4. Sensor studies

For gas-sensing properties, the calcined material was grounded into fine powder and then mixed with α-terpineol to form the paste. This paste was coated onto an ceramic tube substrate (8 mm in length, 2 mm in external diameter and 1.6 mm in internal diameter) provided with platinum wire electrodes for electrical contacts. The thickness of sensing layer was kept at ~30 μm, calculated by means of weight gain method. The coated sensor element was annealed at 500 °C for 1 h to evaporate α-terpineol. To improve the stability and repeatability, the sensor was aged at 350 °C for 5 days in air prior to use. The gas sensing performance of the sensor was studied in a sealed test chamber (300 cm^3) made up of aluminum with a gas inlet and outlet. A nichrome alloy coil placed inside the tube was heated to provide the necessary temperature and a chromel–alumel thermocouple (TC) was used to read the inside operating temperature of the test chamber. The test gases were injected separately into the test chamber through an injection port and their corresponding electrical resistance was measured. The chamber was then purged with fresh air and the experiments were repeated. The electrical resistance of the sensor element in the absence of gas was also measured by means of conventional circuitry in which the load resistor was connected in series with the sensor element. The voltage drop across the sensor element, at a circuit voltage of 10 V, was used to calculate the electrical resistance of the test gases. The sensor response (S) is defined as the ratio of $\Delta R/R_a$ that is the change in resistance of the sensor in air (R_a) and in the test gas (R_g) [13].

$$S = \frac{\Delta R}{R_a} = \frac{(R_a - R_g)}{R_a}$$

The optimum operating temperature, at which the maximum change in the resistance with gas adsorption was observed by plotting sensor response as a function of operating temperature for the test gases. At the optimum operating temperature, the sensor response was measured as a function of various concentrations of test gases and time.

5. Results and discussion

5.1. Thermal analysis

Fig. 1 shows simultaneous TG/DTA thermograms of the precursor sample. The DTA curve showed one endothermic transformation followed by two distinguishable exothermic transformations. The endothermic peak that appeared at about 114 °C is due to the removal of water molecules present in the precursor sample. The first exothermic peak appears at 257 °C is due to the burning nature of peroxo-citro-niobiate with nitrate. The second exothermic peak appears at 417 °C is due to the decomposition of the remaining organic constituents in the precursor. After >500 °C there was no appreciable mass loss that indicates the phase formation. Hence, the precursor sample was kept at 600 °C to get the $InNbO_4$ nanopowder.

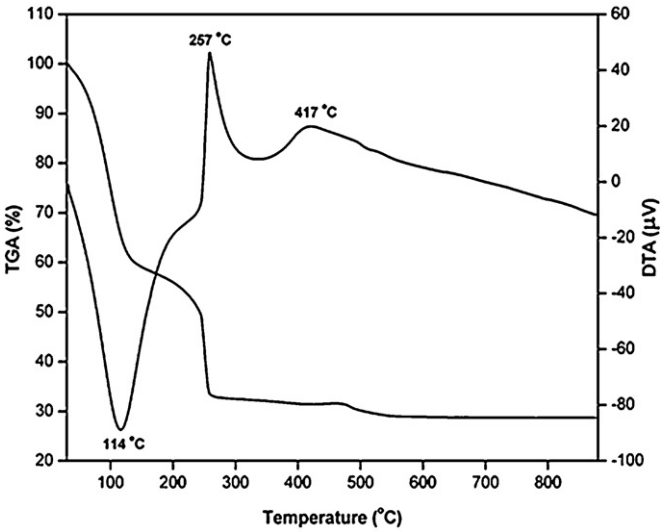

Fig. 1. TG/DTA curves of $InNbO_4$ precursor.

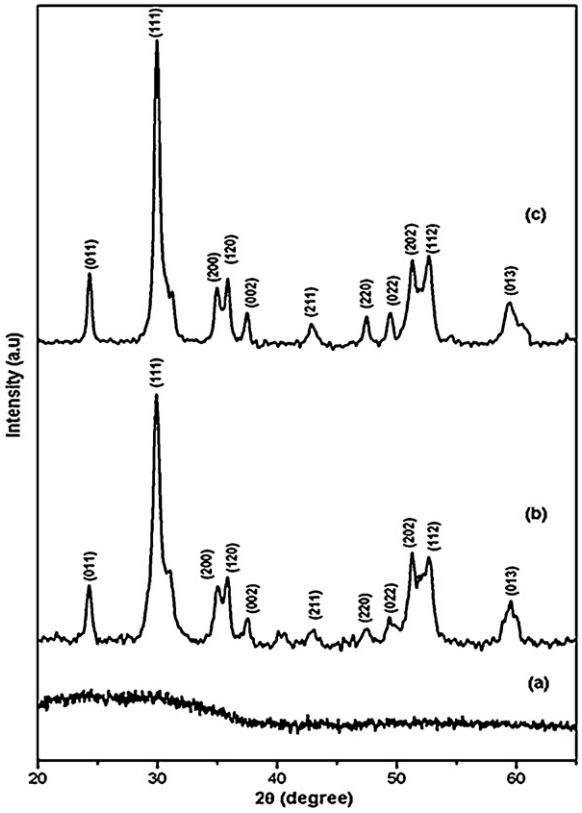

Fig. 2. X-ray diffraction patterns of $InNbO_4$ precursor powder calcined at (a) 400 °C, (b) 500 °C and (c) 600 °C for 2 h.

5.2. X-ray diffraction analysis

Fig. 2 shows X-ray diffraction patterns of $InNbO_4$ powder calcined at different temperatures, 400, 500, and 600 °C for 2 h. The material calcined at 400 °C showed no significant diffraction peaks. The material calcined at 500 °C, exhibited some individual oxide peaks, indicating that the calcinations temperature was still not sufficient. At 600 °C, a single phase $InNbO_4$ was formed with an increase in intensity. The optimum calcination temperature for the formation of a well defined monoclinic phase of $InNbO_4$ was 600 °C. All the peaks coincided with standard JCPDS data (Card No: 33-0619) [14]. The formation of peaks with the line broadening indicated the formation of nanocrystalline particles. The formation of $InNbO_4$ at 600 °C for 2 h was a considerably lower temperature process compared with the same obtained by the conventional solid-state reaction methods [11]. The calculated lattice parameters such as $a = 5.138$ Å, $b = 5.772$ Å and $c = 4.840$ Å was close agreement with the standard lattice parameter values. The average crystalline size of $InNbO_4$ was calculated using Scherrer equation, and it was found to be 15 nm.

5.3. SEM analysis

Fig. 3 shows the typical SEM of the precursor sample calcined at 600 °C for 2 h. The SEM image revealed that the obtained particles were spherical like structures with uniform distribution. The porosity of the material is due to fast expulsion of gas during the synthesis process. It enhances the effective gas sensing properties.

5.4. TEM analysis

The TEM image of the prepared $InNbO_4$ powder calcinated at 600 °C for 2 h is shown in Fig. 4. The image confirms the spherical

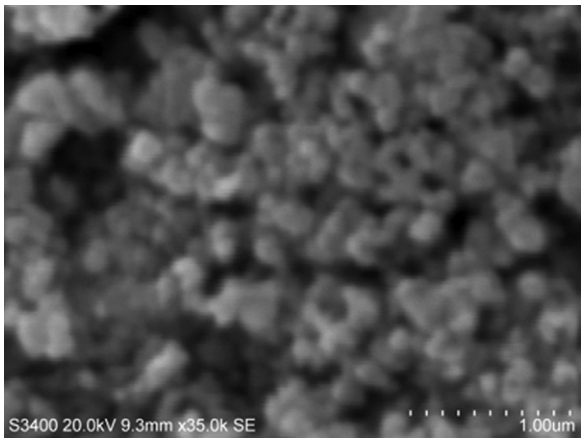

Fig. 3. Scanning electron micrographs of $InNbO_4$ powder obtained at 600 °C.

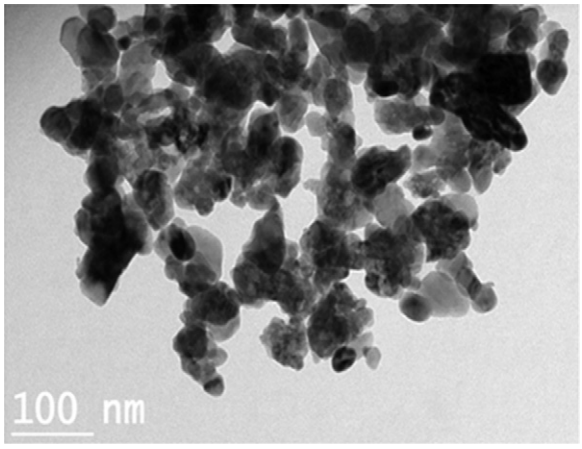

Fig. 4. Transmission electron micrograph of $InNbO_4$ obtained at 600 °C.

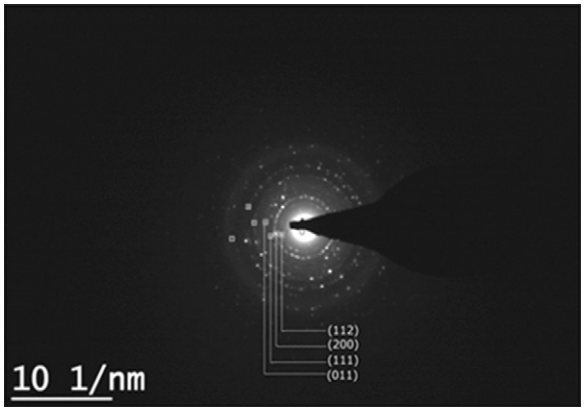

Fig. 5. SAED pattern of $InNbO_4$ nanopowder obtained at 600 °C.

shape of the particles, with uniform distribution. The average diameter of $InNbO_4$ particles was found to be 22 nm. The nanosized materials are desirable to enhance the gas-sensing properties of semiconducting oxides. The particle size estimated from TEM is somewhat grater than calculated from the XRD pattern using Scherrer's formula. The difference might be because the techniques. TEM provides surface topography while X-ray penetrates within and gives the average picture [2].

The selected area electron diffraction (SAED) pattern obtained for the prepared $InNbO_4$ nanopowder as shown in Fig. 5. The diffraction pattern showed that the powder is well crystalline, and the

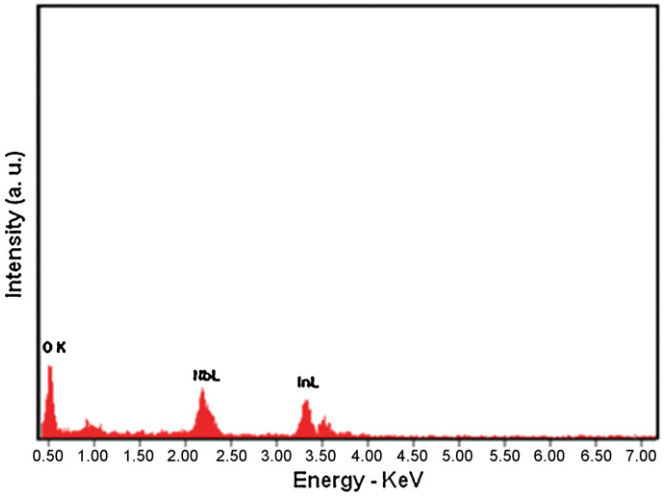

Fig. 6. EDX analysis of $InNbO_4$ nanopowder obtained at 600 °C.

observed rings confirmed the presence of crystal lattice of (2 0 0), (1 1 2), (1 1 1) and (0 1 1) orientation. The observed diffraction rings revealed the monoclinic phase of the sample. This is consistent with the X-ray diffraction analysis.

5.5. Energy dispersive X-ray spectroscopy studies

The composition of the prepared $InNbO_4$ nanopowder was analyzed by EDX as shown in Fig. 6. The atomic % for In, Nb and O was found out from EDX, and it was 17.20, 17.50 and 65.30, respectively, which was very close to the stoichiometric ratio of pure $InNbO_4$. This result is consistent with X-ray diffraction analysis of the sample with phase corresponding to $InNbO_4$.

5.6. Impedance studies

The room temperature complex impedance plot of the prepared $InNbO_4$ sample is shown in Fig. 7. The presence of the semicircular portion corresponding to the higher frequency region is mainly due to the bulk resistance of the material, whereas at the lower frequency region only the linear spike existed, which confirmed the presence of grain boundary effects on the sample. It was also observed that the semicircular portion disappeared with the increase of temperature, which suggests that the bulk resistance of $InNbO_4$ decreased. The resistance of the sample can be calculated

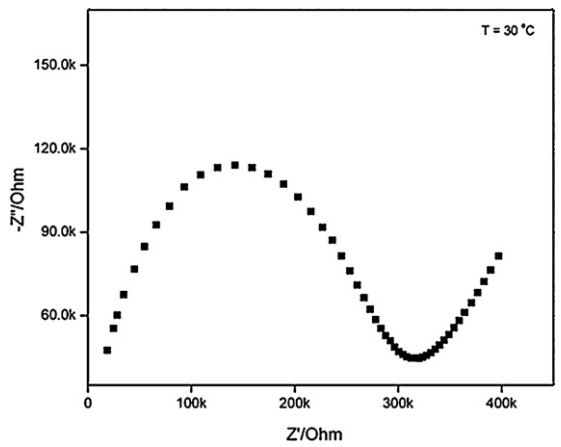

Fig. 7. Impedance spectrum of $InNbO_4$.

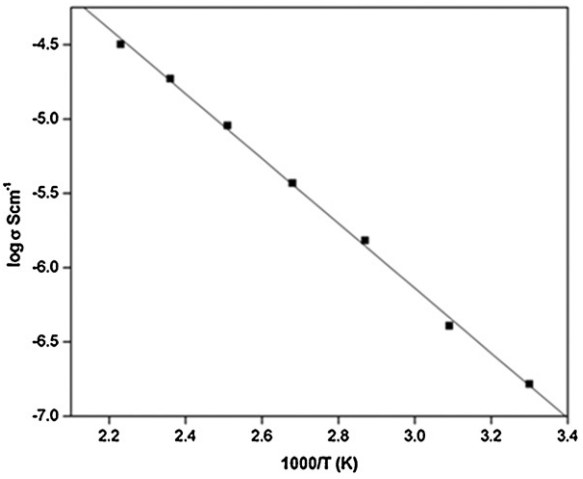

Fig. 8. Arrhenius plot of conductivity of $InNbO_4$.

from the *x*-axis of the complex impedance plot. The electrical conductivity of $InNbO_4$ was calculated following the relation;

$$\sigma = \frac{L}{RA}$$

where σ is the electrical conductivity, L is the thickness of the sample, and A is the area of the sample. Fig. 8 shows the Arrhenius plot of conductivity as a function of temperature in the air for $InNbO_4$ nanopowder. It was observed that the conductivity varied linearly with reciprocal temperatures ($1/T$) as expected for a typical semiconducting material. This semiconducting behaviour of $InNbO_4$ is due to oxygen deficiency [15,16]. From the slope of the plot, the activation energy (E_a) for the conduction process was calculated and was found to be 0.43 eV.

5.7. Diffuse reflection spectra (DRS)

The diffuse reflectance spectra of $InNbO_4$ powder is shown in Fig. 9. The extrapolation of the straight line at zero absorption of the plotting, absorption against wavelength, leads to the absorption edge value (λ) and it was 465 nm. From this, the optical band gap E_g was calculated following the relation [17];

$$E_g = \frac{hc}{\lambda}$$

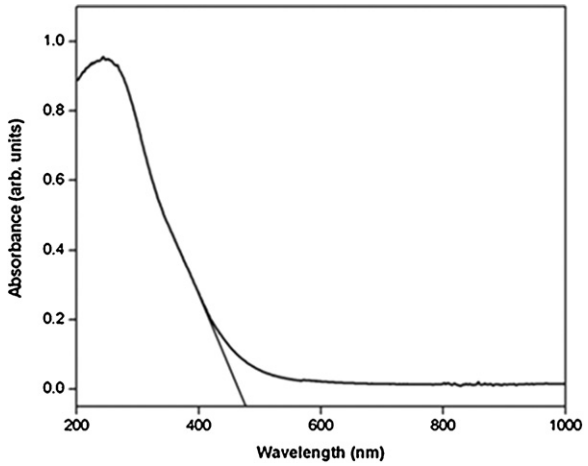

Fig. 9. UV–vis diffuse reflection spectra of nanocrystalline $InNbO_4$.

where h is the Plank's constant (6.602×10^{-34}), C is the velocity of light (3×10^{8}), and it was found to be 2.66 eV, which is greater than the same obtained by high temperature solid state reaction method [6].

5.8. BET specific surface area studies

The specific surface area of $InNbO_4$ nanopowder calcined at 800 °C was measured by nitrogen adsorption BET method, and it was 39.24 m^2/g.

6. Gas sensing behaviour

6.1. Gas sensitivity with operating temperatures

$InNbO_4$ nanopowder was subjected to gas sensor studies with test gases like LPG, NH_3, and C_2H_5OH by measuring sensor response as a function of various operating temperatures (Fig. 10). The $InNbO_4$ sensor showed the highest sensitivity with LPG (0.97) and NH_3 (0.70) gas at 300 °C and for ethanol (0.46) at 325 °C. It is well known that the sensing mechanism of semiconductor gas sensor materials is a surface controlled process. The change in resistance is mainly caused by the adsorption and desorption of oxygen on the surface of sensing materials. When sensor is exposed to the air, oxygen is adsorbed on the sensor surface. It traps electrons from the conduction band of the sensor material to produce negatively charged chemisorbed oxygen such as O_2^-, O^{2-} and O^-, respectively. The chemisorbed oxygen species depended strongly on the operating temperature. At relatively lower operating temperature O_2^- preferentially adsorbed on the surface of $InNbO_4$ and the sensitivity of the material was consequently, low. As the temperature increased, O^- and O^{2-} were commonly chemisorbed. The adsorption of O^- was the most interesting process in sensors, because these oxygen ions were more reactive and thus made the material more sensitive to the presence of reducing gases. When the reducing gases were inleted, the overall reaction of LPG, NH_3 and C_2H_5OH chemisorbed oxygen species as follows [18–20];

$$C_nH_{2n} + 2 + 2O^- \rightarrow H_2O + C_nH_{2n}{:}\ O + e^-$$

$$C_nH_{2n}{:}\ O + O^- \rightarrow CO_2 + H_2O + e^-$$

$$2NH_3 + 3O^-_{(ads)} \rightarrow NO + 3H_2O + 3e^-$$

$$C_2H_5OH + O_2 \rightarrow CH_3CHO + H_2O$$

$$CH_3CHO + O^-_{(ads)} \rightarrow CO_2 + H_2O + e^-$$

electrons released from the above reaction enter into the conduction band of sensor material resulting in change of resistance. When the concentration of LPG, NH_3 and ethanol gas in an air was the same, enhanced sensitivity was obtained at 300 °C, owing to the amount of chemisorbed oxygen ions reaching the maximum at that temperature. Ethanol is maximum response was found to shift towards the higher operating temperature 325 °C. This may be attributed to the availability of sufficient adsorbed ionic species of oxygen on the sensor surface which react most effectively with ethanol molecules at this particular temperature. Beyond this optimal operating temperature, the response decreased due to progressive desorption of all previously adsorbed oxygen ionic species. This might also be one of the possible reasons for the decrease in response at higher temperatures.

6.2. Sensor sensitivity with gas concentrations

Fig. 11 showed the sensor response of $InNbO_4$ as a function of various concentrations of test gases at their optimum operating temperatures. The sensor response increased with increases in the concentration of test gases and attained almost a maximum response at 500 ppm for all three gases. The response of a sensor depends on removal of adsorbed oxygen molecules by reaction with a target gas and generation of electrons. For a small concentration of gas, exposed on a fixed surface area of a sample, there is a lower surface coverage of gas molecules on the surface and hence lower surface reaction occurred. An increase in gas concentration increases the surface reaction due to a larger surface coverage. A further increase in surface reaction will be gradual until the saturation point on the coverage of molecules is reached.

6.3. Sensor response with time

The sensor response with time was studied to know performance of the sensor. The response time is defined as the time taken to reach the maximum response when the requisite amount of test gas is introduced into the test chamber keeping the sensor at the optimum operating temperature. The recovery time, is the time taken to return to the initial resistance value when the gas is turned off at the optimum operating temperature from its

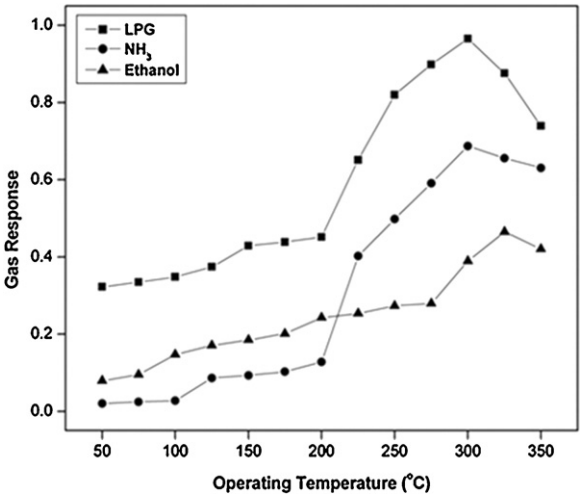

Fig. 10. Gas sensing characteristics of $InNbO_4$ sensor as a function of various operating temperatures for LPG, NH_3 and C_2H_5OH gases.

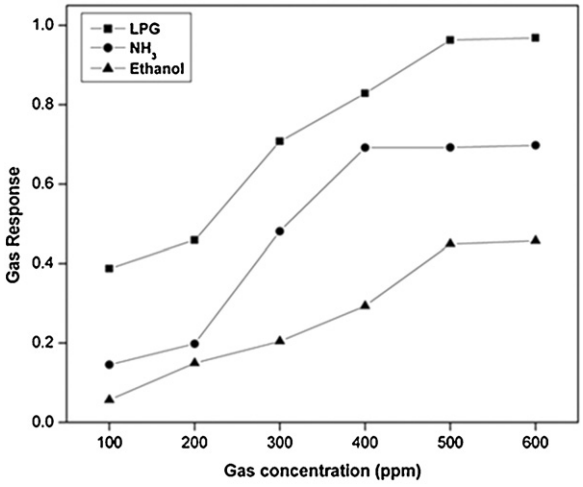

Fig. 11. Sensitivity of $InNbO_4$ sensor with the different concentrations of LPG, NH_3 and C_2H_5OH at their optimum operating temperatures.

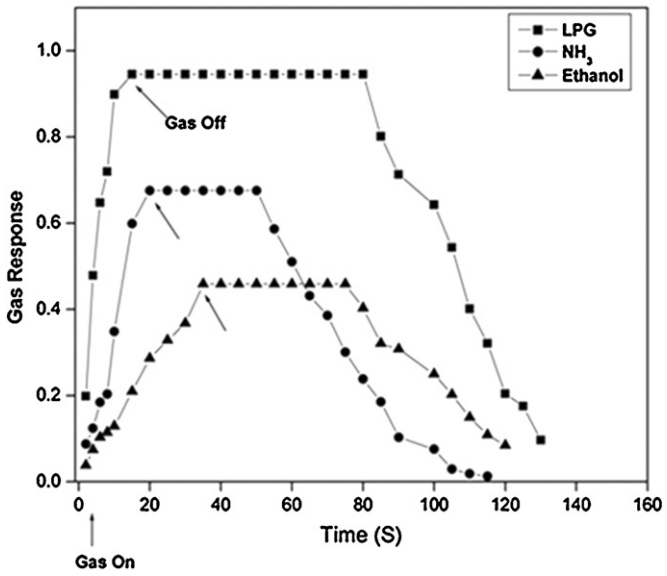

Fig. 12. Response of $InNbO_4$ sensor as a function of time at their optimum operating temperatures for LPG, NH_3 and C_2H_5OH gases.

maximum response. Fig. 12 shows the sensor response with time for LPG, NH_3 and ethanol gas at the optimum operating temperature of 300 °C for LPG, and NH_3 and 325 °C for ethanol, respectively. It can be seen that LPG gas attained maximum response within 14 s, and it was 19 s and 35 s for NH_3 and ethanol, respectively. However, their recovery times were less than 124 s, 114 s and 99 s, for LPG, NH_3 and ethanol gases, respectively.

7. Conclusions

Nanocrystalline $InNbO_4$ powder was prepared by comparatively low temperature niobium citrate complex process. Typical monoclinic structure of $InNbO_4$ was obtained at 600 °C for 2 h was confirmed by XRD and electron diffraction pattern of TEM analysis. SEM image showed spherical particles with uniform grain size distribution. TEM analysis revealed that the average particle diameter was 22 nm. EDX was in good agreement with the nominal composition, and the diffuse reflection spectra showed that optical band gap was 2.66 eV. The temperature dependent conductivity plots of the sample obeyed the Arrhenius relation. The sensitivity analysis showed that $InNbO_4$ has a better response to LPG, NH_3 gases at an operating temperature of 300 °C than C_2H_5OH (325 °C). The response times of LPG, NH_3 and C_2H_5OH were about 14, 19 and 35 s, respectively.

Acknowledgements

The authors thank Dr. G.N. Chaudhari, Dept. of Chemistry, Shri Shivaji Science College, Amravati (India) for providing the gas sensing measurement facility. The authors also thank the Dept. of Metallurgical and Materials Science, Indian Institute of Technology (I.I.T.) Madras for providing the TEM facility.

References

[1] J. Xu, X. Wang, G. Wang, J. Han, Y. Sun, Electrochem. Solid-State Lett. 9 (2006) H103–H107.
[2] V.D. Kapse, S.A. Ghosh, G.N. Chaudhari, F.C. Raghuwanshi, Talanta 76 (2008) 610.
[3] G. Korotcenkov, I. Boris, V. Brinsari, Yu. Lychkovsky, G. Karkotsky, V. Golovanov, A. Cornet, E. Rossingol, J. Rodriguez, A. Cirera, Sens. Actuators B 103 (2004) 13.
[4] M. Ivanovskaya, P. Bogdanov, Sens. Actuators B 53 (1998) 44.
[5] V. Romanovskaya, M. Ivanovskaya, P. Bogdanov, Sens. Actuators B 56 (1999) 31.
[6] Z. Zou, J. Ye, H. Arakawa, Mater. Res. Bull. 36 (2001) 1185.
[7] A.L. Petre, J.A. Perdigon-Melon, A. Gervasini, A. Auroux, Catal. Today 78 (2003) 377.
[8] Z. Zou, J. Ye, H. Arakawa, Chem. Phys. Lett. 332 (2000) 271.
[9] Z. Zou, J. Ye, K. Sayama, H. Arakawa, Nature 414 (2001) 625.
[10] S. Wongsaenmai, R. Yimnirun, S. Ananta, Mater. Lett. 61 (2007) 2426.
[11] S. Wongsaenmai, R. Yimnirun, S. Ananta, J. Mater. Sci. 42 (2007) 3754.
[12] R.N. Das, P. Pramanik, Mater. Lett. 46 (2000) 7.
[13] S.V. Jagtap, A.V. Kadu, V.S. Sangawar, S.V. Manorama, G.N. Chaudhari, Sens. Actuators B 131 (2008) 290.
[14] PCPDFWIN Version 2.4, JCPDS-ICDD, 2003.
[15] K.I. Gnanasekar, V. Jayaraman, E. Prabhu, T. Gnanasekaran, G. Periaswami, Sens. Actuators B 55 (1999) 170.
[16] V.V. Atuchin, I.E. Kalabin, V.G. Kesler, N.V. Pervukhina, J. Electron Spectrosc. Relat. Phenom. 142 (2005) 129.
[17] S. Esther Dali, M.J. Chocklingam, Mater. Chem. Phys. 70 (2001) 73.
[18] P.P. Sahay, R.K. Nath, Sens. Actuators B 133 (2008) 222.
[19] S.K. Biswas, P. Pramanik, Sens. Actuators B 133 (2008) 449.
[20] M.R. Vaezi, S.K. Sadrnezhaad, Mater. Sci. Eng. B 140 (2007) 73.